Available online at www.sciencedirect.com
SCIENCE DIRECT®
Tectonophysics 376 (2003) 19–35
TECTONOPHYSICS
www.elsevier.com/locate/tecto

From geometry to dynamics of microstructure: using boundary lengths to quantify boundary misorientations and anisotropy

John Wheeler[a,*], Z. Jiang[b], D.J. Prior[a], J. Tullis[c], M.R. Drury[d], P.W. Trimby[e]

[a] *Department of Earth Sciences, University of Liverpool, Liverpool L69 3GP, UK*
[b] *Department of Geology and Geophysics, Yale University, P.O. Box 208109, New Haven, CT 06520-8109, USA*
[c] *Department of Geological Sciences, Brown University, Providence, RI 02912, USA*
[d] *Geodynamics Research Institute, Faculty of Earth Sciences, Utrecht University, P.O. Box 80.021, 3508 TA Utrecht, The Netherlands*
[e] *HKL Technology ApS, Majsmarken, DK-9500 Hobro, Denmark*

Received 16 January 2003; accepted 22 August 2003

Abstract

The microstructure of a quartzite experimentally deformed and partially recrystallised at 900 °C, 1.2 GPa confining pressure and strain rate 10^{-6}/s was investigated using orientation contrast and electron backscatter diffraction (EBSD). Boundaries between misoriented domains (grains or subgrains) were determined by image analysis of orientation contrast images. In each domain, EBSD measurements gave the complete quartz lattice orientation and enabled calculation of misorientation angles across every domain boundary. Results are analysed in terms of the boundary density, which for any range of misorientations is the boundary length for that range divided by image area. This allows a more direct comparison of misorientation statistics between different parts of a sample than does a treatment in terms of boundary number.

The strain in the quartzite sample is heterogeneous. A 100×150 μm low-strain partially recrystallised subarea C was compared with a high-strain completely recrystallised subarea E. The density of high-angle (>10°) boundaries in E is roughly double that in C, reflecting the greater degree of recrystallisation. Low-angle boundaries in C and E are produced by subgrain rotation. In the low-angle range 0–10° boundary densities in both C and E show an exponential decrease with increasing misorientation. The densities scale with $\exp(-\theta/\lambda)$ where λ is approximately 2° in C and 1° in E; in other words, E has a comparative dearth of boundaries in the 8–10° range. We explain this dearth in terms of mobile high-angle boundaries sweeping through and consuming low-angle boundaries as the latter increase misorientation through time. In E, the density of high-angle boundaries is larger than in C, so this sweeping would have been more efficient and could explain the relative paucity of 8–10° boundaries.

The boundary density can be generalised to a directional property that gives the degree of anisotropy of the boundary network and its preferred orientation. Despite the imposed strain, the analysed samples show that boundaries are not, on average, strongly aligned. This is a function of the strong sinuosity of high-angle boundaries, caused by grain boundary migration. Low-angle boundaries might be expected, on average, to be aligned in relation to imposed strain but this is not found.

* Corresponding author.
E-mail address: johnwh@liverpool.ac.uk (J. Wheeler).

0040-1951/$ - see front matter
doi:10.1016/j.tecto.2003.08.007

Boundary densities and their generalisation in terms of directional properties provide objective measures of microstructure. In this study the patterns they show are interpreted in terms of combined subgrain rotation and migration recrystallisation, but it may be that other microstructural processes give distinctive patterns when analysed in this fashion.

Keywords: Rock texture; Quartz; Dynamic recrystallisation; Electron backscatter diffraction (EBSD); Deformation; Misorientation

1. Introduction

Microstructures of deformed rocks reflect the processes and conditions of deformation. In principle, measurements of microstructures should allow inferences to be made about those processes and conditions. Many basic observations we make are qualitative, and inferences are broad—for example, lattice distortions might be taken to imply the operation of dislocation creep. Further insight is gained from quantitative observations such as quartz *c*-axis patterns (measured optically, by X-ray goniometry or by electron backscatter diffraction (EBSD)) which can be used to infer active slip systems and, arguably, to constrain temperatures of deformation. Simple measures of grain and subgrain size may relate to stress levels. Microstructural observations on experimentally deformed quartz aggregates have been used to define different dislocation creep regimes characterised by different mechanisms of dynamic recrystallisation (Hirth and Tullis, 1992). Our interest is in refining dynamic models for microstructure development on the basis of quantitative measurements of microstructure that, until recently, were hard to make. This contribution shows how electron backscatter diffraction (EBSD) can be used to quantify and display the populations of different types of grain and subgrain boundaries in deformed material and how it may be used to refine models for microstructural development. A method of numerical analysis, based on boundary length statistics rather than grain/subgrain size statistics, is discussed. We show that the boundary length statistics have certain numerical advantages, and that they relate directly to models for the generation and destruction of boundaries during dynamic recrystallisation.

We analysed a single experimentally deformed sample of quartzite using EBSD. In contrast to natural samples, the starting material, deformation history and conditions are relatively well constrained. The sample strained heterogeneously, so contains subareas with different finite strains and degrees of dynamic recrystallisation that can be compared with each other. EBSD data were combined with the results of image analysis to give a map of domains of crystal orientation (grains or subgrains) separated by boundaries across which misorientations can be calculated. Numerical summaries of these boundary maps have been used to suggest models for aspects of microstructural evolution.

2. Methodology

2.1. Experimental details

Black Hills quartzite is a strain-free metaquartzite with equant grains (average size 100 μm) and consists of ~ 99% quartz with ~ 1% feldspars and oxides and an average porosity up to ~ 1–2% by volume. Sample BA-42 with 0.17 wt.% water added was deformed in dislocation creep regime 3 (Hirth and Tullis, 1992) at 900 °C and 1.2 GPa confining pressure, and is characterised by grain boundary migration recrystallisation. These conditions are similar to those of the sample CQ-78 which was studied by Hirth and Tullis (1992). The added water causes softening, and leads to microstructures comparable to those formed in dry quartzites at higher temperatures; it appears that the water-related species that causes the softening equilibrates quickly with the quartz (Post and Tullis, 1998). The spatially averaged strain rate was $10^{-6}\,s^{-1}$ but there was a strain gradient between the two pistons over a distance of 5 mm, from weakly deformed protolith (partially recrystallised) near one piston to completely dynamically recrystallised grains near the other. The sample was shortened by 60% in about 5 days. Assuming a purely oblate strain (in accord with the symmetry of the experimental apparatus), we have average finite strains $Z=0.4$ and $X=Y=(0.4)^{-1/2}=1.58$, so that $X/Z=3.95$ for the sample as a whole.

2.2. Measurement methodology

EBSD gives a method for determining the complete lattice orientation at a point in a crystalline material, using a scanning electron microscope (Adams et al., 1993; Prior et al., 1999). In the case of quartz, it is equivalent to measuring the *c*-axis (as in the optical universal stage method) and at least one other crystal direction, for example, an *a*-axis (which cannot be measured optically). The complete lattice orientation is essential for determining the misorientation between two crystal lattices—two quartz grains or subgrains may have subparallel *c*-axes, which would suggest a low-angle boundary between them, but the *a*-axes may be substantially different. This is one advantage of using EBSD rather than optical measurements. Optical studies would also be virtually impossible on the small subgrains present in the deformed sample.

In the last 10 years, EBSD has become automated, in the sense that hardware and software are available to enable a regular array of points to be analysed and the results displayed as a map and analysed in a variety of ways (Adams et al., 1993). Such maps would be appropriate for our investigation and could be used in future work; however, at the time our data were gathered, automatic EBSD analysis of quartz gave rise to substantial misindexing problems. Algorithms which calculate crystal orientation from the patterns of backscattered electrons are becoming reliable for complex structures such as minerals, but automation should still be approached with caution (Trimby et al., 2002).

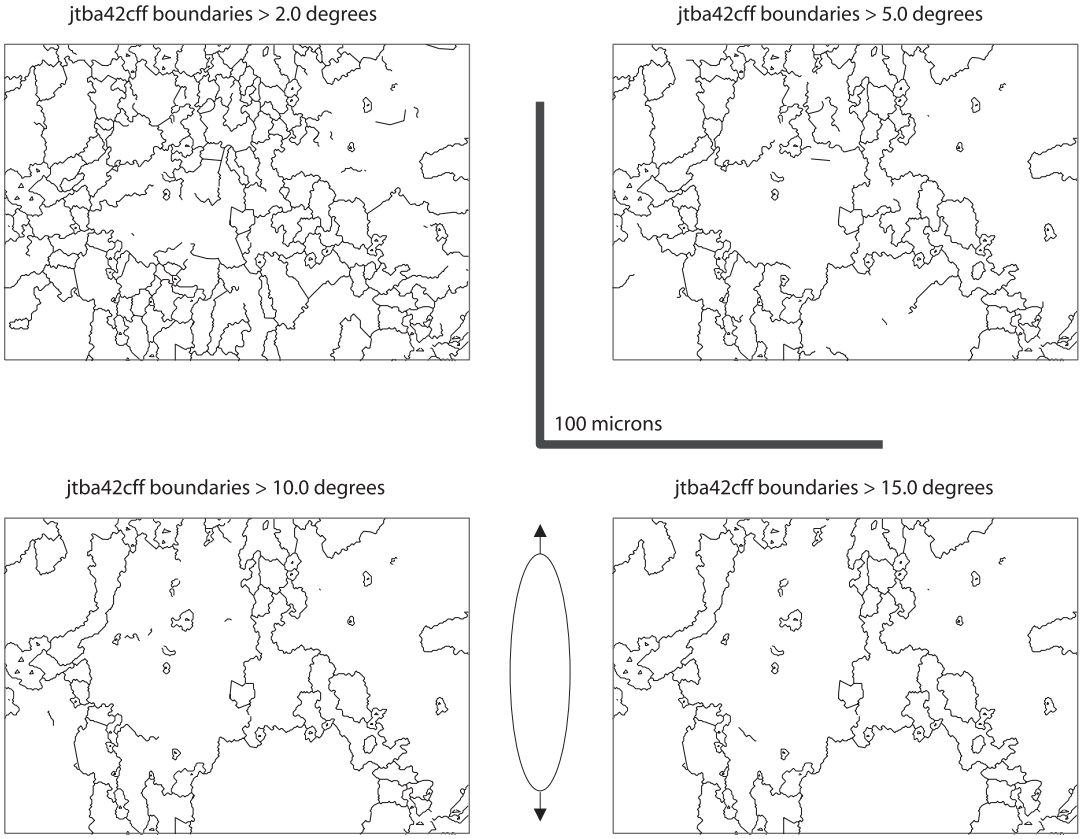

Fig. 1. Boundary maps from subarea C. Each map shows all those boundaries whose misorientations are above a threshold value. Thin lines mark the boundaries of holes in the slide. Ellipse shows the calculated finite strain ellipse for the whole sample (which overestimates strain in subarea C).

Instead, we analysed a discrete set of points from each subarea of the sample, but first needed to decide where to make measurements and how many to make. First, orientation contrast (OC) images from each subarea were collected using a Phillips XL30 scanning electron microscope at Liverpool. These show grey scale contrasts between domains of differing orientation. Grain boundaries and subgrain boundaries are equally apparent (Trimby and Prior, 1999), in contrast to optical images. By chance, some boundaries may not show in the OC image because there is no grey scale contrast (Prior et al., 1996). OC images cannot themselves be used to deduce crystal orientation, but can be used as a guide to what shapes and size of orientation domains there are. An image analysis program (Bartozzi et al., 2000) was used to pick out boundaries between orientation domains. This initial boundary map was then used as a guide to where to put EBSD measurement points, which were analysed using Channel 3.1 software. More EBSD points than domains were used and this leads to a revision and refinement of the boundary map (Bartozzi et al., 2000). The result is a map with domains that are assumed internally homogeneous (one analysis point per domain).

Each boundary between domains has a misorientation that can be calculated from the EBSD measurements on either side. Three numbers are required to define a misorientation, for example, two numbers to define the direction of the rotation axis and one more number to define the angle of rotation required to bring one lattice into alignment with the other. Because of crystal symmetry, there are several possible angles and rotation axes that can be used to rotate one quartz crystal lattice into the same orientation as another. By convention, the minimum angle is chosen from all the possibilities. This minimum angle is strictly called the disorientation (MacKenzie and Thompson, 1957; Vorhauer et al., 2003) but is commonly referred to as the misorientation (Bunge and Weiland, 1988; Pospiech et al., 1986; Wheeler et al., 2001). Boundary maps can then be displayed (e.g. Fig. 1) showing any subset of boundaries selected on the basis of their misorientation angles (Adams et al., 1993). The boundaries themselves are only as detailed as the pixel spacing of the orientation contrast image will allow, but nevertheless these maps can provide insight into how quartz deforms and recrystallises.

3. Quantitative data analysis—review

In this section we discuss the methods available to extract and display statistical information from the boundary maps.

Grain size and subgrain size have sometimes been used to infer stress levels (palaeopiezometry): there is direct evidence and a collection of theories behind this procedure (e.g. Derby, 1990; Edward et al., 1982; Gleason and Tullis, 1993). To use such techniques, grain and subgrain boundaries must be distinguished from each other. Strictly, this distinction involves knowing the misorientations across all boundaries and defining a "cutoff" misorientation separating grain and subgrain boundaries. The cutoff angle is not well known for any mineral but estimates vary between 5° and 15°, and for quartz it is normally greater than 10° (White, 1977). In many studies the distinction has been made optically, giving two measures of size. This is not objective and, as Figs. 1 and 2 show, there is a whole hierarchy of misorientations defining the boundary network, so there is far more information available than just two numbers (Trimby et al., 1998). Moreover, the misorientation is an objective descriptor of a boundary, regardless of whether it is a grain or subgrain boundary. The analysis of such a hierarchy within a single sample, and comparisons between samples, provides information to constrain recrystallisation models (Trimby et al., 1998) and could eventually lead to a "unification" of grain and subgrain size palaeopiezometric techniques, as well as illuminating other aspects of microstructural evolution (e.g. Heidelbach et al., 2000). One aim of this contribution is to discuss different methods of quantifying that hierarchy. To do this, we need to take into account the length-related features of the boundary network, and the (mis)orientation-related features. A variety of methods exists, which we have found helpful to classify in Table 1. Sections 3.1 and 3.2 give the context that leads to the statement of our method in Section 3.3.

3.1. Length-related statistics

Consider a network of boundaries where that network is not classified in any way. We could count the number of boundary segments between triple junctions: this is not very useful on its own (column (a) of Table 1). We could define domains completely

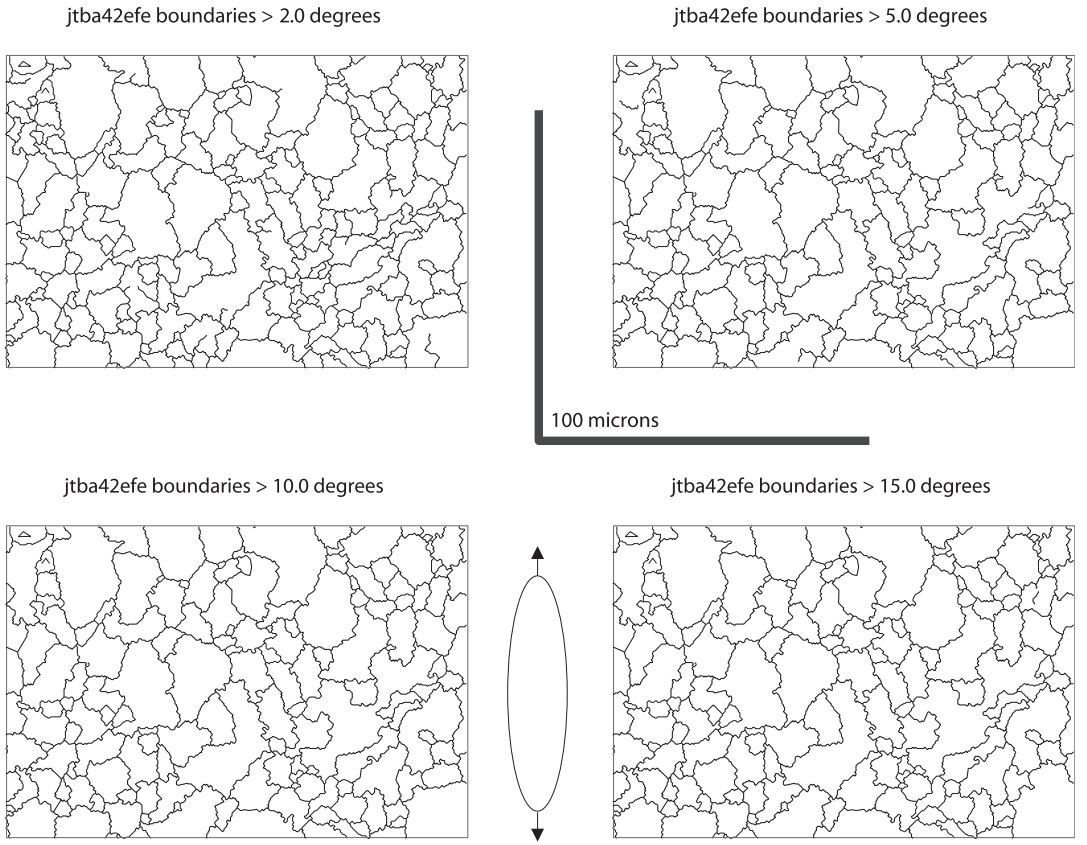

Fig. 2. Boundary maps from subarea E with the same explanation as Fig. 1, except now the sample finite strain underestimates the strain in subarea E.

enclosed by boundaries and measure the areas of these domains (column (b)). This enables us to analyse the spectrum of grain areas, and is a common task performed in image analysis. Alternatively, we can measure the boundary length per unit area of the map (e.g. Heilbronner and Tullis, 2002) to give a quantity with dimensions of m^{-1} (column (c)). This will scale with the inverse of the average domain size in a broad sense, but not in detail.

3.2. (Mis)orientation-related statistics

Now consider generalising those statistics to situations where the boundaries are characterised by their misorientation. The concepts of grain and subgrain size can be generalized to that of an average domain size defined for each misorientation angle θ (Trimby et al., 1998). There, a domain was defined as an area in 2D entirely surrounded by boundaries of misorientation $>\theta$—the name "domain" will be used in this specific sense in this contribution. Plotting the average areas of such domains for different θ is an objective method of quantifying the microstructure and of displaying differences in microstructure, e.g. differences in the amount of recrystallisation between low and high strain microstructures in a mylonitic quartz vein (Trimby et al., 1998). However, it is hard to visualise how the domain distribution would evolve through time, in any model for recrystallisation. For instance, consider the sketch in Fig. 3. Here we envisage a change in microstructure through time by amalgamation of two small subgrain walls of 7° into one of 14°. The whole figure used to be a single domain bounded by $\theta>12°$, now it is two domains. There has been a major reduction in domain size $\theta>12°$ though a minor change in actual geometry. The issue is that domains

Table 1
Classification of different ways of quantifying misorientation data, to illustrate how those methods relate to each other

Nature of boundary subdivision	Weighting		
	(a) By boundary number	(b) By enclosed domain volume in 3D (areas of enclosed domains in 2D)	(c) By boundary area per unit volume in 3D (or length per unit area in 2D)
None, or on a simple selection criterion		Many image analysis techniques (Frese et al., 2003)	Heilbronner and Tullis, 2002
By misorientation angle	Faul and Fitz Gerald, 1999; Field and Adams, 1992; Fliervoet et al., 1997	Trimby et al., 1998	This contribution
By all three misorientation parameters	Pospiech et al., 1986		Adams et al., 1987; Bunge and Weiland, 1988; Pospiech et al., 1986
By three misorientation parameters and two boundary orientation parameters			Adams, 1986

Each box gives examples of a method, not a complete list of studies. Empty boxes indicate approaches that have not, to our knowledge, been used.

are defined on the basis of *topology*. A domain of $\theta>12°$ has to be surrounded by boundaries of $\theta>12°$. If any segment of that boundary becomes $<12°$, suddenly the domain is radically changed in size. In addition, a 2D map of any sort cannot give reliable information on topology and connectivity in the third dimension; therefore, the definition of domains may be somewhat artificial. These issues are relevant for any approach that lies in column (b) of Table 1.

An alternative method for displaying misorientations is to take all pairs of neighbouring (touching) grains or subgrains, calculate the misorientation angles and represent their distribution graphically, e.g. as a histogram (Faul and Fitz Gerald, 1999; Hughes et al., 1997; Randle, 1993; Trimby et al., 1998; Wheeler et al., 2001). Such distributions do not capture all aspects of the misorientation, since they do not indicate any information about rotation axes. The misorientation distribution function (MODF) describes the probability density for the occurrence of a specified misorientation between adjacent (neighbouring) measurement points (Pospiech et al., 1986) and requires three dimensions to represent, since a misorientation is defined by three independent numbers. It is common, though, for the phrase "misorientation distribution" to be used in relation just to misorientation angle (e.g. Fliervoet et al., 1997). The MODF as proposed by Pospiech et al. (1986) may be used to summarise geometric relationships which are, in detail, not directly comparable between different studies. For example, it may be used to assign equal weight to each misorientation derived from a pair of touching grains (e.g. Faul and Fitz Gerald, 1999; Hughes and Hansen, 1997). In such a strategy, the user decides where the boundaries are, and makes measurements on either side accordingly. Such analyses lie in column (a) of Table 1. Alternatively, a regular grid of analysis points can be used (e.g. Haessner et al., 1983). If the grid spacing is comparable to or larger than the size of some grain or subgrain structure, the MODF from this analysis will not necessarily resemble that derived from neighbouring grains or subgrains. Conversely, if the grid spacing is much smaller than the size of some grain or subgrain structure, then every boundary will be picked up by the MODF, but in some cases multiply as many pairs of analysis points will be separated by one boundary. In this case, the MODF will be weighted by the length of each boundary. Again, this might differ from the MODF in which each boundary is given unit weight, and the distinction is important so we put it in a separate column (c) in Table 1. In detail, there are many issues related to grid point spacing (Pennock et al., 2002), but here we proceed by stating that *in principle* the length-weighted MODF is a property of the microstructure, not of the method used to determine it.

Bunge and Weiland (1988) define the "physical MODF" through weighting the misorientation according to the area fraction of grain boundaries with that

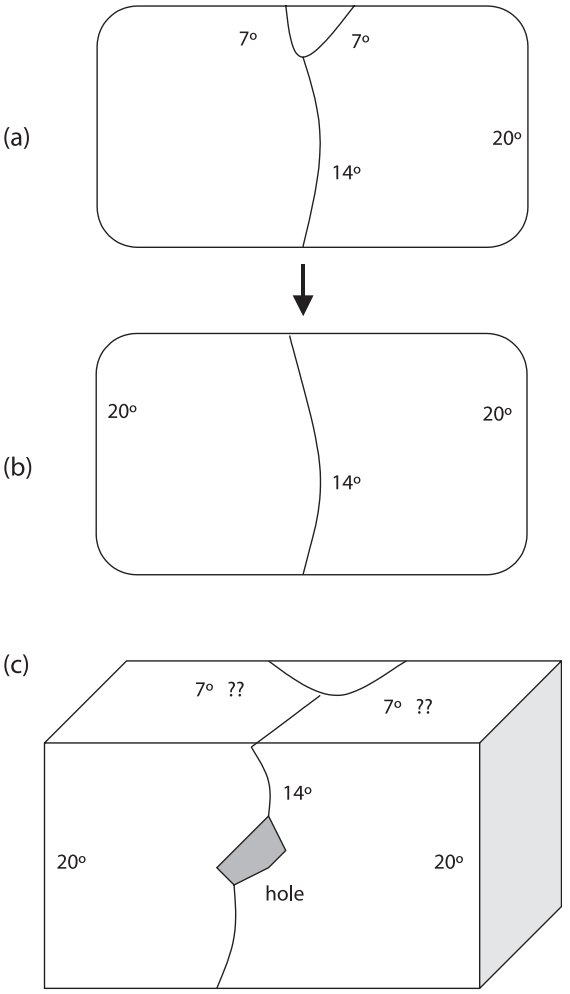

Fig. 3. Cartoons showing topological problems with defining grains as entities. In (a) there is one 12° domain (defined as an area completely surrounded by boundaries of at least 12°). A small change in boundary geometry in (b) leads to a large change in the number and size of 12° domains (the single domain is split in two). The distribution of boundary lengths will register just a small change. Objective identification of domains is difficult for other reasons: does the 14° boundary continue across the hole in (c)?

misorientation. If boundaries of particular misorientations are in some way favoured in a microstructure, so they have a proportionately larger area, this approach will give different statistics to that in which each boundary is given equal weight. This idea can be extended yet further to take into account boundary orientation as well as misorientation. This gives rise to the functions ψ and ϕ (Bunge and Weiland, 1988) or the intercrystalline structure distribution function (ISDF) (Adams, 1986). For a boundary near a given orientation and misorientation, this gives the surface area per unit volume. It differs from the physical MODF in two ways: first, it takes into account boundary orientation; secondly, it is defined in terms of boundary area per unit volume (measured in units of $(\text{length})^{-1}$), rather than boundary area fraction relative to total boundary area (dimensionless). The latter distinction is mathematically trivial but significant to us. The ISDF can be normalised and displayed in dimensionless form (e.g. (Adams et al., 1990), or given in units of $(\text{length})^{-1}$ (e.g. Field and Adams, 1992). The MODF (which can be calculated from the ISDF) is also commonly displayed in dimensionless form (Adams, 1993), which is sufficient for many purposes but discards the absolute length-scale information. The dimensionless MODF is useful when, for example, it is compared with distributions of misorientations from pairs of grains taken at random (not necessarily touching), because differences between the two types of distribution can give information on processes (e.g. Bunge and Weiland, 1988; Heidelbach et al., 2000; Wheeler et al., 2001).

In summary, the ISDF contains information on the surface area per unit volume for different types of boundary. It is not sensitive to topological problems but does contain length-scale information. It also relates directly to the boundary energy per unit volume (Eq. (53) of Bunge and Weiland, 1988). The essence of this relationship is that

$$\begin{aligned}&(\text{boundary energy per unit volume})\\&\quad=(\text{boundary energy per unit area})\\&\qquad\times(\text{boundary area per unit volume})\end{aligned}$$

where the boundary energy per unit area is an intrinsic property of the boundary, in principle determinable (e.g. for MgO (Saylor et al., 2000)). In detail, this is complex because the boundary energy may depend on all five parameters defining the boundary orientation and misorientation. We mention it here because no such comparable relationship can be written between grain size and boundary energy per unit volume. This illustrates that the description

of microstructures in terms of boundary density statistics can be advantageous in terms of their link to physical properties.

3.3. Analysis presented here

In this contribution, we use a much-simplified version of the ISDF in which we discuss surface area per unit volume purely in terms of misorientation angle. This simple version of boundary statistics is sufficient to show interesting patterns. It is defined by the function $a(\theta)$ where
(area per unit volume of boundaries with misorientation angles lying between θ and $(\theta + d\theta)) = a(\theta)d\theta$.

In practice, we instead measure the length per unit area of boundaries in a section plane. We call this $b(\theta)$ to emphasise that it is not the same function, though it is closely related. There are stereological relations between $a(\theta)$ and $b(\theta)$. In an isotropic structure, the relationship is

$$a(\theta) = (4/\pi)b(\theta)$$

(Weibel, 1980), so that $b(\theta)$ would underestimate $a(\theta)$ by 21%. In anisotropic structures such as the ones in this study, the relationships are more complex and we do not attempt to estimate $a(\theta)$. In general, several section planes should be cut to determine $a(\theta)$. In this contribution, we illustrate the form of $b(\theta)$ for two subareas and compare these distributions. The histograms displaying $b(\theta)$ are derived from finite areas of the sample. We judge that these areas are representative of the "local" microstructure. Larger areas would have given more representative statistics, but would give rise to other problems since the sample shows a strain gradient.

4. Boundary data

We analysed two subareas of 100×150 μm from sample BA-42: BA-42C (a low strain part, called C for short) and BA-42E (high strain, called E for short). These both come from a single SYTON-polished thin section that was cut parallel to Z, thus showing the maximum strain ratio. Fig. 4 shows that C contains parts of about five original grains (some of their original diameters in this section cut were somewhat less than the 100 μm average). Fig. 5 illustrates the total lengths of boundary, with bins in the histograms defined as ranges of misorientation. We split the histograms into two parts; there is so much low-angle boundary density in both samples that it is difficult to see the density of high-angle boundaries if they are all plotted together.

Comparing Fig 5a for C and E shows that the >10° boundaries have roughly twice the density in E as in C. We interpret this as a reflection of progressive recrystallisation to finer average grain size during the approach to a steady-state microstructure. Both histograms show high densities in the range 60–90° and a steep drop-off to 105°, primarily due to the influence of crystal symmetry on misorientation distribution; randomly oriented equant quartz grains show a comparable pattern (Wheeler et al., 2001). Fig. 6 shows the theoretical prediction of the frequency of different misorientations to be expected in a random array of quartz crystallites, in which each boundary between neighbouring grains is counted once. If there is no bias of boundary lengths towards particular misorientations, we expect the boundary density histogram to have identical appearance, except for the y-axis being presented in units of $(\text{length})^{-1}$. Thus, some broad aspects of the histograms can be explained in terms of the crystallography of quartz, not in terms of specific microstructural processes. The link between boundary density histograms and theoretical misorientation patterns illustrates an advantage of using boundary density rather than domain area. The size of domains increases without limit as θ approaches 105°; moreover, even for a random distribution of equant grains, it is not straightforward to predict theoretically how average domain size would depend on θ. In contrast, a preliminary assessment of the boundary density is easy. Statistical tests for whether the high-angle histograms differ in detail from those for a random distribution could be applied but are outside the scope of this contribution.

Details of boundaries <10° are shown in Fig. 5b and c and show marked differences. There is an abundance of very low-angle boundaries (subgrain walls) in both C and E, with boundary density decreasing with increasing θ. However, the drop-off is much more marked in E. In C, the line density in the range $2° < \theta < 4°$ is about three times less than in $0° < \theta < 2°$ and this exponential decrease carries to

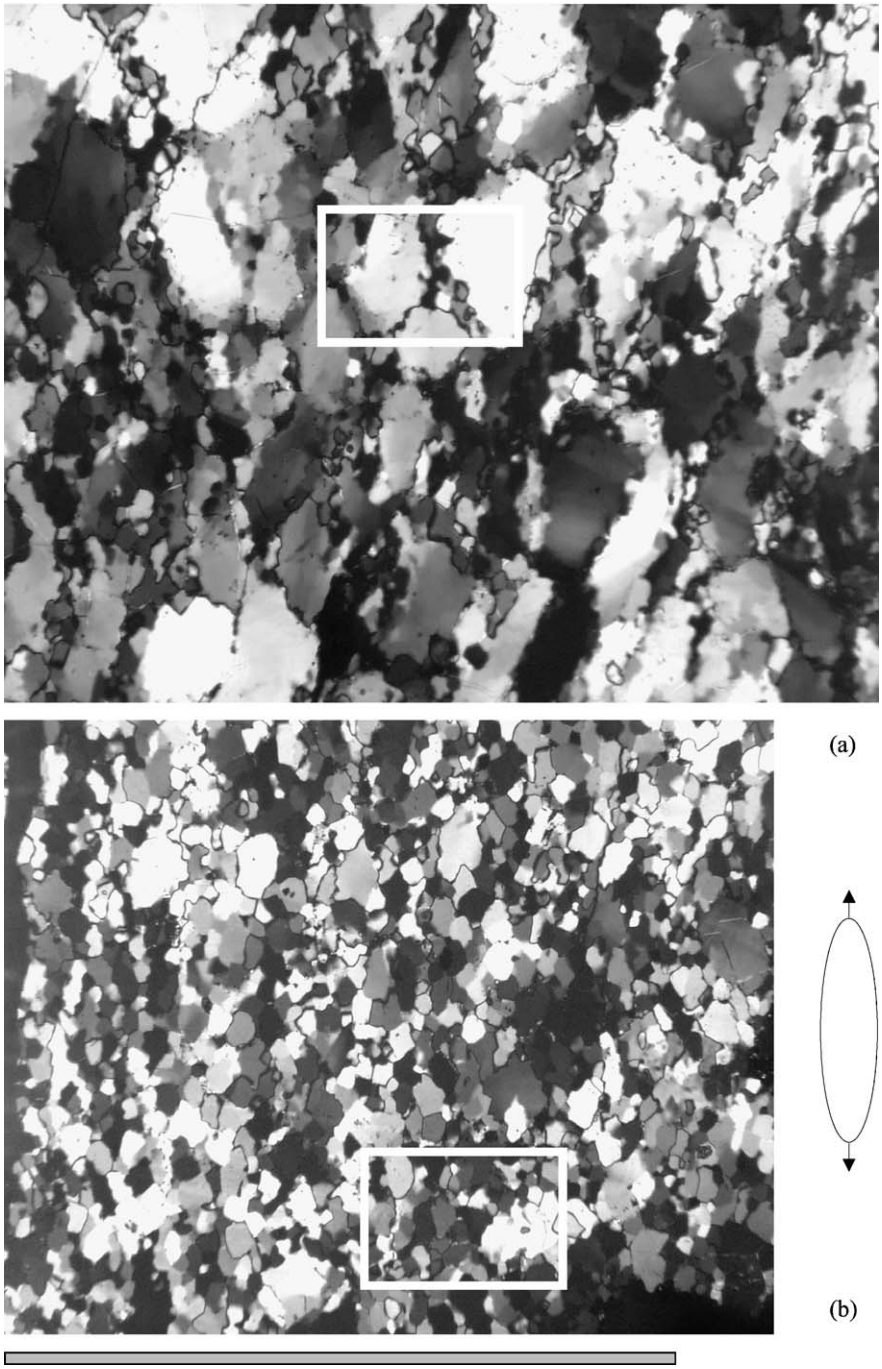

Fig. 4. Optical images of BA-42 (crossed polars) showing (a) low strain region with subarea C (white box), and (b) a high strain region with subarea E. Scale bar is 500 μm. Ellipse shows the calculated finite strain ellipse for the whole sample (which overestimates strain in subarea C).

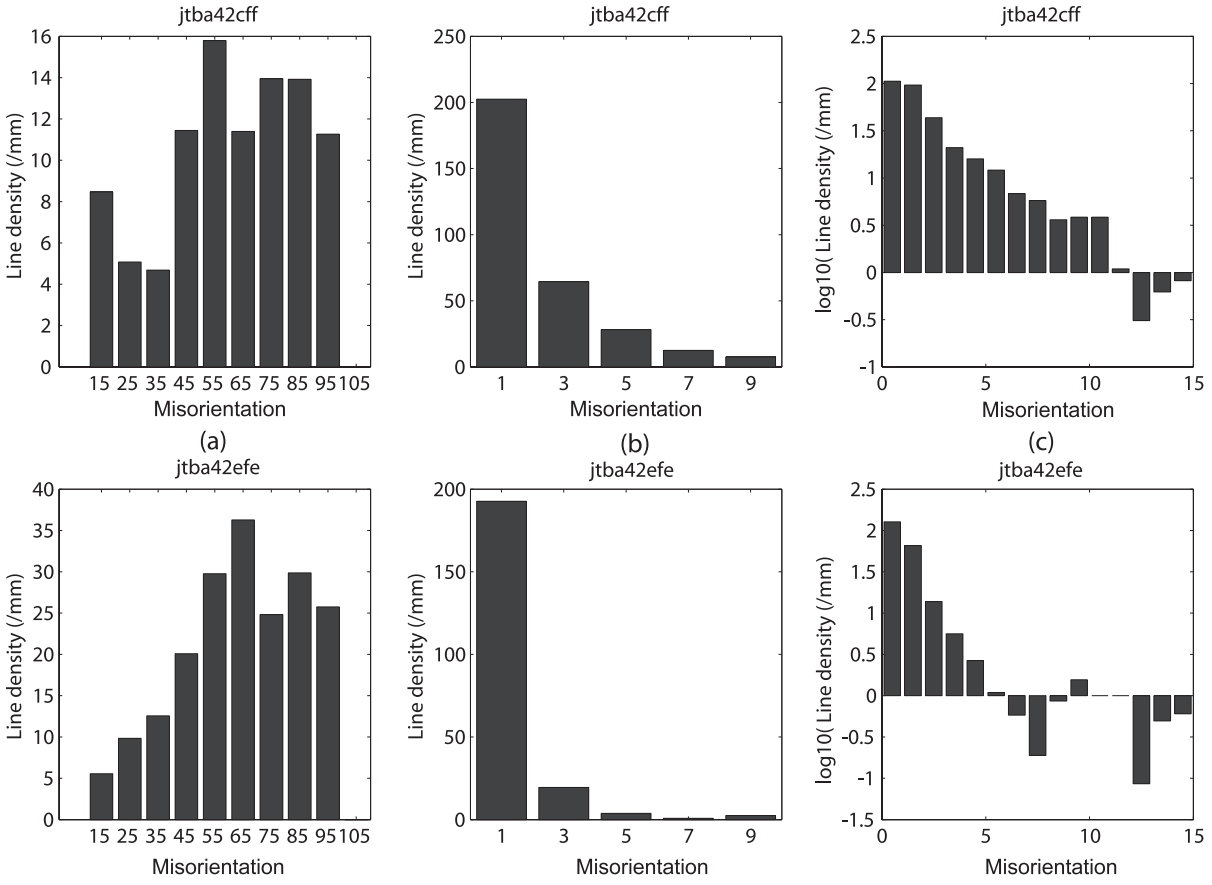

Fig. 5. Boundary length histograms for C and E. For each subarea, we show (a) high angle boundaries ($10° < \theta < 105°$), (b) a more detailed binning of low-angle boundaries ($2° < \theta < 10°$) and (c) a logarithmic display of $0° < \theta < 15°$.

higher misorientations. In E, the line density in the range $2° < \theta < 4°$ is about seven times less than in $0° < \theta < 2°$, so there are proportionately fewer higher-angle boundaries. The logarithmic plots (Fig. 5c) show a linear trend for low angles, though note that the high-angle bins relate to small boundary lengths and are therefore less significant. Errors in indexing EBSP patterns automatically are 0.75° or less (Lassen, 1996). Small uncertainties in crystal orientation lead to large uncertainties in calculated misorientation axes for low-angle misorientation angles (Prior, 1999), but we do not deploy axis information here. The errors in calculating misorientation angles themselves are no greater for low-angle misorientations than for high angle ones. We expect errors in the calculated misorientation angles to be of the order of 1–1.5°. Since we are dealing with the bulk statistics of many calculated misorientations, we do not think these errors make a major difference to the patterns we document.

So, there is an approximate linear relationship between $\ln(b)$ and θ in both subareas, which we write as

$$\ln(b(\theta)) = \ln(b_0) - \theta/\lambda$$

which implies

$$b(\theta) = b_0 exp(-\theta/\lambda)$$

where b_0 and λ are constants for each microstructure. These constants are defined purely by the geometry of the microstructure. λ is a sort of geometric decay constant. An approximate best-fit straight line

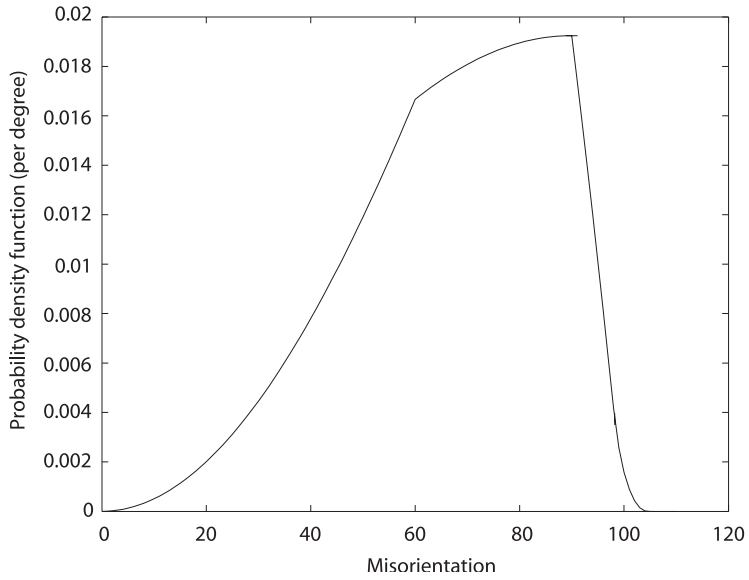

Fig. 6. Misorientation distribution for a set of randomly oriented quartz grains.

through the low-angle parts of Fig. 5c shows that λ is approximately 2° for subarea C and 1° for E.

5. Interpretation of boundary data

There are some similarities between these observations on a quartz rock deformed experimentally in pure shear and previous observations on a natural quartz mylonite deformed in simple shear. Trimby et al. (1998) used EBSD to characterise two subareas of a sheared quartz vein. In a low strain, 0.6 × 0.6 mm area, the microstructure was heterogeneous and included both relict grains and more thoroughly recrystallised matrix; a nearby high strain area was more homogeneous. Fig 7 shows histograms of boundary number versus misorientation for both subareas. Trimby et al. (1998) subdivided the low strain area into "relict" and "matrix" but here we have amalgamated these two datasets to enable more direct comparison with the new data we present here. In the low strain zone, boundary numbers decrease gently towards 15°, whilst in the high strain zone numbers drop off more quickly to 10°. These patterns mimic the reduction in boundary length versus misorientation angle for the low and high strain parts of the experimentally deformed sample, bearing in mind that the histograms of Fig. 7a–c do not take into account the boundary lengths. Fig. 7d shows domain sizes as a function of misorientation. The average area of domains in the relict grains increases smoothly up to a misorientation of 10° (a continuous hierarchy) whilst it flattens off at ca. 2° in the higher strain recrystallised matrix and in the high strain subarea (a discrete hierarchy). This flattening off is again compatible with a relative dearth of 4–12° boundaries in the recrystallised matrix and in the high strain subarea. Although data collection and display techniques differ between this study and that of Trimby et al. (1998), so that we do not propose a more detailed comparison, there do seem to be common patterns.

Whether microstructural characteristics are expressed as domain sizes or as boundary densities (advocated here) as a function of misorientation, their evolution must depend on the formation and evolution of subgrain walls and on grain boundary migration. An improved understanding of these processes is important because they relate to the approach to a steady-state microstructure, and have implications for strength evolution and rheology. First consider a single sample. The lowest angle boundaries must be subgrain walls (TEM provides direct evidence, e.g. Fig. 6 of Hirth and Tullis, 1992), formed continuously by recovery. We will assume here that any boundary up to at least 10°

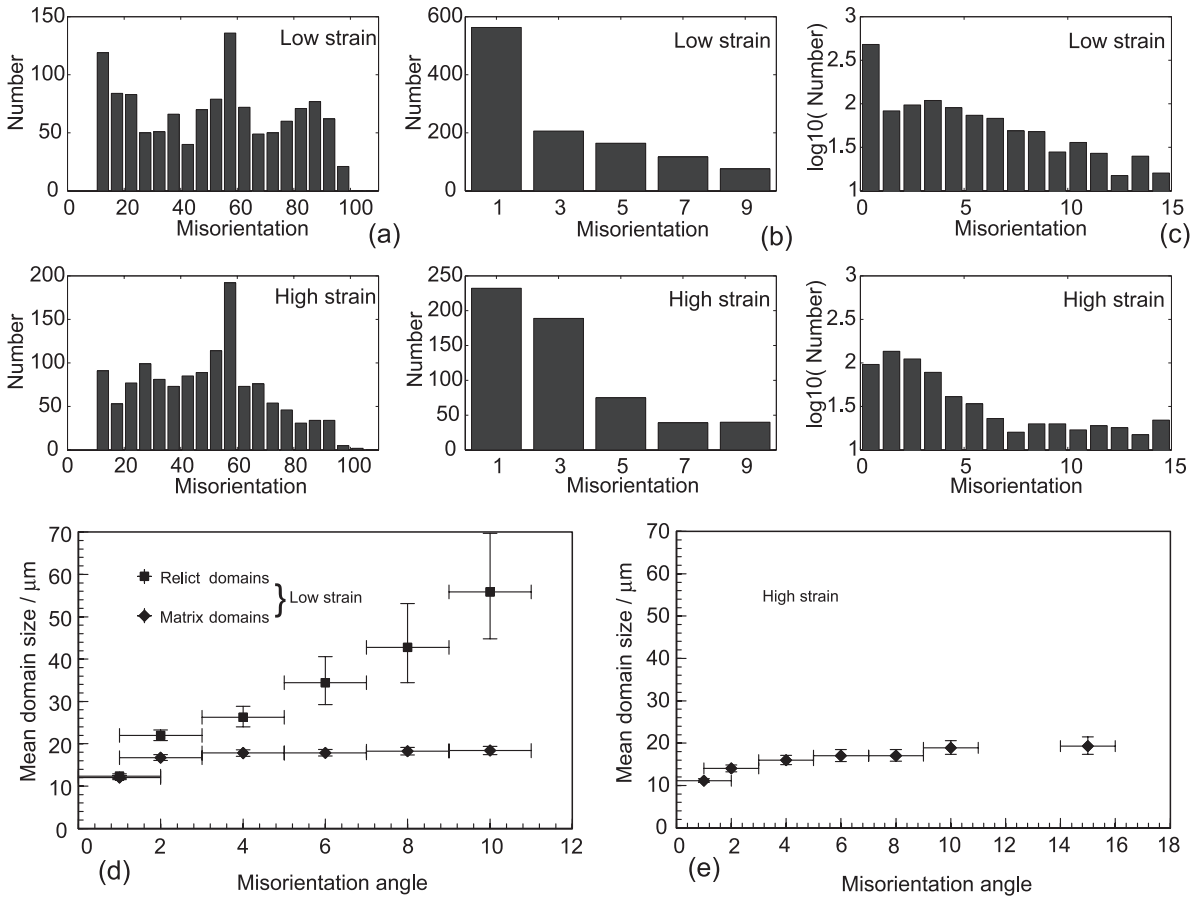

Fig. 7. Boundary number histograms for a naturally sheared quartz rock (Trimby et al., 1998). (a) to (c) are histograms for low and high strain zones laid out in the same fashion as (a) to (c) in Fig. 5 to enable comparison. (d) and (e) show the sizes of domains as a function of misorientation, with error bars.

misorientation (i.e. the range over which Eq. (1) applies) is, in quartz, a subgrain wall. The standard model for subgrain rotation recrystallisation serves as a starting point for our discussion. In this model, subgrain walls will accumulate dislocations through time and increase their misorientations (e.g. Poirier, 1985). This accumulation will, in the absence of other effects, cause any pattern on a misorientation histogram to move to increasing angles (cf. Fig. 13 of Trimby et al., 1998). Ongoing strain will continue to produce dislocations and new subgrain walls. Within this model, it is reasonable to suppose that high-angle subgrain walls are on average older than low-angle ones, since they will have had longer to incorporate dislocations. Fig. 5 shows, however, that the line density of (old) higher-angle subgrain walls is much less than that of low angle ones.

There may then be another process at work that destroys subgrain walls—the obvious candidate is grain boundary migration (Poirier, 1985) and again TEM offers direct evidence for this process in comparable quartzite samples (Fig. 6 of Hirth and Tullis, 1992). Grain boundary migration is driven by plastic strain energy differences, including that of subgrain walls (Poirier, 1985, p. 182). A migrating high-angle boundary may consume low-angle boundaries as it sweeps through the region containing them. The misorientation across the high-angle boundary must be modified as it sweeps across subgrains of slightly different orientations and regions of bent lattice. Mis-

orientation angles are not additive, but it is sufficient for our model to postulate that most high-angle boundaries remain high angle during their movement. Suppose, for example, that a boundary of misorientation angle θ sweeps across and incorporates a subgrain wall of misorientation ψ. The final misorientation angle depends on the misorientation axes of the two boundaries. However, the extreme values possible are $\theta+\psi$ and $\theta-\psi$. If one boundary is high angle, say 50°, and the other low angle, say 4°, the resultant misorientation angle must be at least 46°. So, on the whole, high-angle boundaries will remain high angle as they migrate.

Suppose then that a microstructure contains mobile high-angle boundaries. In a small interval of time dt, suppose that a fraction dt/τ of an area is swept in this way. Then, after time t, the fraction of unswept area is $\exp(-t/\tau)$—this is analogous to the radioactive decay law. We remark that this exponential form mimics the relative paucity of higher-angle (?older) subgrain walls. In radioactive decay, the constant τ relates to the half-life of the radioactive element. If subgrain walls also have a "half-life", this would influence the measured geometric constant λ. A short half-life would mean that subgrain walls are commonly consumed by a migrating boundary before they can grow to high misorientation angles: a small τ implies a small λ.

The microstructure in C is clearly heterogeneous, with relict grains showing as large areas bounded by swathes of smaller grains on the >15° map (Fig. 1). However, we have no objective way of defining what is relict and what is new. The boundaries of the relict grains are blurred, especially when we look at the map including low-angle boundaries (>2° map, Fig. 1). Bearing this in mind, we now compare the low strain dataset C with high strain E. Care must be taken because although they come from a single sample, the higher strain in E means the strain rate was slightly faster. Nevertheless, we will assume (as is often done for natural examples) that C shows microstructures that would have evolved to those like E. In E, the density of subgrain walls drops off more quickly with misorientation (λ is smaller). One possibility is that the half-life of subgrain walls in E is less than in C. The half-life will depend on how often any particular point is swept by a mobile migrating boundary. The mobility is itself a function of misorientation (Lloyd and Freeman, 1994). So the half-life of a low-angle boundary will be governed by both the density and mobility of higher-angle boundaries. It is obvious from (Figs. 1, 2 and 5) that there are more boundaries of all misorientations above 25° than there are in C—the continual migration of this dense network may help to keep the 7–15° misorientation interval swept almost clean of boundaries. In fact, the density of >10° boundaries in C is 96/mm, and that in E is 194/mm, roughly double. We note that doubling the density of high-angle boundaries in E is associated with halving the decay constant λ from 2° to 1°. Trimby et al. (2000) compared microstructures from wet and dry salt and found that faster grain boundary migration in wet salt led to a misorientation pattern like that in E, whereas slower migration in dry salt produced one like C. Taken together, the quartz and salt data are compatible with a model in which either an increased density or an increased mobility of grain boundaries lead to more effective "sweeping" of a plastically strained microstructure.

This more rapid destruction of low-angle boundaries is one explanation of why the densities of 7–15° boundaries in E are lower than those in C, but we need to explain how the densities of *higher*-angle boundaries in E have increased over those in C. There are at least two methods of generating increased densities of high-angle boundaries: the bulging of existing high-angle boundaries, and the evolution of low-angle subgrain walls towards higher misorientations, leading eventually to the loss of dislocation substructure in the boundary (Urai et al., 1986). These two processes may be related, when a subgrain wall forms at the neck of a bulging boundary. These two processes are sufficient to explain the production of high-angle boundaries.

In summary, our dynamic model involves

1. development of subgrain walls by recovery
2. gradually increasing misorientation across those walls with time
3. increasing (gradual or sudden?) mobility of boundaries as misorientation increases
4. scavenging of low-angle boundaries by more mobile higher-angle boundaries
5. bulging of existing high-angle boundaries, as well as production of high-angle boundaries from subgrain walls, leads to increased density of high-angle boundaries
6. increased scavenging rate leads to shorter half-life of low-angle boundaries
7. possible approach to steady state (Means, 1981).

We cannot yet assign numbers to the rates of these processes, but in principle dynamic models could be tested against observations via prediction and observation of boundary density.

6. Boundary orientation and measures of anisotropy

In this section we show how boundary density can be generalised to give a directional quantity, a measure of anisotropy. If a microstructure is characterised in terms of grains, then their shapes as well as areas may carry microstructural information. Shapes may reflect strain, though this is complicated by recrystallisation. The boundary density, being a scalar, does not indicate any anisotropy, but it does relate closely to a directional quantity. Suppose we wish to examine the anisotropy of a set of boundaries which, taken all together, can be approximated by N short straight line segments in total, with $(x^{(n)}, y^{(n)})$ being the vector describing the magnitude and direction of the n^{th} segment. If we sum these vectors along a given boundary, we obtain merely the vector joining the start and end points, which is not very helpful, as well as being ambiguous in sign. Instead, consider the 2×2 symmetric tensor quantity

$$D_{ij} = \sum_{n=1}^{N} T_{ij}^{(n)} / (\text{image area})$$

where the tensor **T** is for each of the N line segments is given by

$$\mathbf{T} = \begin{bmatrix} x^2 & xy \\ xy & y^2 \end{bmatrix} (x^2 + y^2)^{-1/2}$$

D is invariant with respect to changes in the coordinate system. It is also basically unaltered if we change the (arbitrary) way in which a boundary is approximated by straight line segments. Specifically consider a completely straight boundary. It could be represented by a single vector or by two parallel vectors each with half the length, and so on—but whatever choice is made, the final value of **D** is the same. The link between **D** and the boundary density B is simply

$$B = tr\,\mathbf{D} = D_{11} + D_{22}$$

The tensor **D** has two eigenvalues, and the direction of the eigenvector linked to the maximum eigenvalue indicates any preferred direction of boundary alignment, in the following way. Imagine a boundary network made of rectangles of side length p parallel to x and q parallel to y. Then

$$\mathbf{D} = \begin{bmatrix} 1/q & 0 \\ 0 & 1/p \end{bmatrix}$$

If the rectangles have their long axes parallel to x, then $p>q$, and $D_{xx}>D_{yy}$. The maximum eigenvalue is in the direction of the long axes of the rectangles. If D_1 is the maximum eigenvalue, then the ratio of eigenvalues $R=D_1/D_2$ indicates the intensity of boundary alignment. For the case of the rectangles, $R=p/q$, so is simply the length/width ratio of the rectangles. For an isotropic boundary network, the ratio would be 1. This analysis is related to an approach to solving a separate geological problem, that of estimating the strain from a set of linear markers which have been reoriented (Wheeler, 1989)—but in the present context, **D** is best thought of as a combined *description* of the boundary density and anisotropy. Other measures of anisotropy might, for example, involve defining closed domains ("grains") and defining best-fit ellipses to their shapes. As in the definition of domain size, this approach will be prone to topological issues. Moreover, the approach we present here tends to highlight different aspects of the microstructure, as we now discuss.

Table 1 shows the eigenvalues and eigenvectors of **D** for various misorientation ranges in subareas C and E. The angle of the maximum eigenvector is measured relative to the extension direction in each subarea. If the boundary network was initially isotropic, and deformed passively, this angle is expected to be zero. The last column, the sum of eigenvalues, is equal to the boundary density and can be checked against, for example, Fig. 5a. Table 2 shows that it is uncommon for any range of boundaries to show much anisotropy, despite the fact that a 60% shortening means that the bulk strain ratio should be 3.95. This is a surprising result that may be explained as follows.

In subarea C, the optical image (Fig. 4a) shows quite elongate old grains. There is an irregular pattern to the directions of anisotropy according to Table 2, but the highest angle boundaries show a preferred orientation

Table 2
Anisotropy of boundary networks, examined by grouping boundaries into intervals of 10° misorientation range

Angular range	D_1 (/mm)	D_2 (/mm)	Angle from extension direction	Ratio	D_1+D_2 (/mm)
jtba42cff					
0–10	161.7	153.5	98.1	1.05	315.2
10–20	4.7	3.7	48.8	1.26	8.5
20–30	2.7	2.4	17	1.16	5.1
30–40	2.8	1.9	44.8	1.45	4.7
40–50	6.0	5.5	23.2	1.09	11.4
50–60	8.4	7.4	171.7	1.14	15.8
60–70	6.9	4.5	137.8	1.53	11.4
70–80	8.0	5.9	177.6	1.36	13.9
80–90	7.5	6.4	2.7	1.17	13.9
90–100	6.1	5.1	2.9	1.20	11.3
jtba42efe					
0–10	110.3	108.8	54.2	1.01	219.1
10–20	2.9	2.7	174.2	1.08	5.5
20–30	5.4	4.4	29	1.22	9.8
30–40	6.9	5.7	121.8	1.21	12.6
40–50	11.0	9.1	144.7	1.22	20.1
50–60	16.0	13.8	146.9	1.16	29.8
60–70	19.1	17.2	16	1.12	36.3
70–80	13.2	11.7	53.2	1.13	24.8
80–90	15.9	14.0	174.9	1.14	29.9
90–100	13.5	12.2	6.2	1.11	25.8

The extension direction runs up and down in Figs. 1–6. D_1 and D_2 are the maximum and minimum eigenvalues of the tensor **D**.

roughly parallel to the extension direction: they may be relict original grain boundaries reoriented by strain. However, the high-angle boundaries defined by EBSD are very sinuous (Fig. 1), due to the onset of grain boundary migration. The boundary analysis takes into account all this sinuosity, and shows that there are significant lengths of boundary in all orientations. A ''smoothed'' boundary network would show more anisotropy. Low-angle boundaries (<10°) are also virtually isotropic in C and E, implying that the initial recovery of plastic strain into subgrain walls is not *on average* influenced by the overall stress or strain fields, or by the lattice orientation of the relict grains in C.

In subarea E, high-angle boundaries are again sinuous, but here even the overall grain shapes are not particularly elongate, which can be explained by the general ease of grain boundary migration in Regime 3 (Hirth and Tullis, 1992). The boundary anisotropy is most developed in the range 20–50° but the alignment is not close to the bulk extension direction; the highest angle boundaries are aligned closer to the extension direction.

These examples show that the tensor **D** can shed light on how isotropic a boundary network is, and that this may not accord with a subjective visual assessment of a boundary map. In particular, **D** may prove to be a useful indicator of boundary sinuosity, alongside other measures (e.g. the PARIS factor (Heilbronner and Tullis, 2002)).

7. Discussion

We have shown that EBSD in conjunction with identification of boundaries and their misorientations can provide quantitative measures of microstructure, which then beg explanation in terms of processes. We propose a boundary density analysis technique that can be used in parallel with or instead of other approaches that involve defining the areas of domains, or counting the number of boundaries. Though we used a procedure involving image analysis of orientation contrast images as well as EBSD to produce boundary maps, the method is equally applicable to EBSD maps produced automatically on a grid of points. Although we apply this technique to a study of a deformed material, it could be used to characterise any microstructure, for example, those produced by grain growth; it could also be deployed in further study of the possibly fractal nature of grain (and subgrain?) boundaries (Takahashi and Nagahama, 2000). We find it useful to form conceptual models of microstructural evolution in terms of boundary density, because it is the boundaries that control many aspects of microstructural evolution, not the grains themselves.

Although the boundary density is a useful characterisation of microstructure, and is sufficient to help us interpret microstructure in this contribution, it is limited by being an average property for the studied area. For example, it averages all heterogeneities such as core and mantle structures that are present in C (Fig. 1). Other methods such as domain size analysis or linear intercept analysis can be used to distinguish the variations in domain size and extract further information, bearing in mind the potential problems discussed earlier. Thus, there are advantages and disadvantages to all the various methods of quantify-

ing microstructure. It is a matter of scientific judgement which of these will be most appropriate in any particular study. Note also that the raw data for such studies will always be from some kind of regular arrangement of points with characteristic spacing (whether this is an orientation contrast image defined by pixels, or an EBSD map). This spacing is likely to bias the identification of boundaries. At the moment, we suggest that comparison of datasets of different sorts, or even of the same type but at different spacing, should be treated with caution.

In dynamic recrystallisation of a quartzite at elevated temperatures, we show that there is an abundance of low-angle boundaries that drops off exponentially as misorientations approach 10°. This drop off is more extreme in more recrystallised regions. It is superimposed on an overall increase of high-angle boundary density with increasing strain. The two phenomena may be linked if we postulate mobile high-angle boundaries constantly sweeping through the dynamically recrystallising microstructure, cleaning out distributed plastic strain and low-angle boundaries. As generalised concepts such models are already established (Urai et al., 1986; White, 1977) but the quantitative approach we advocate here will help to tie down the forms of interaction between processes, and the parameters involved, ultimately enabling more reliable deductions of deformation conditions in the Earth from the frozen products of that deformation.

Acknowledgements

JW, ZJ and DJP were funded by NERC grant GR3/11768. JT was funded by NSF EAR 0106859. M. Bartozzi is thanked for allowing us to use his image analysis programs.

References

Adams, B.L., 1986. Description of the Intercrystalline Structure Distribution in polycrystalline materials. Metallurgical Transactions. A, Physical Metallurgy and Materials Science 17, 2199–2207.

Adams, B.L., 1993. Orientation imaging microscopy—application to the measurement of grain-boundary structure. Materials Science & Engineering. A, Structural Materials: Properties, Microstructure and Processing 166, 59–66.

Adams, B.L., Morris, P.R., Wang, T.T., Willden, K.S., Wright, S.I., 1987. Description of orientation coherence in polycrystalline materials. Acta Metallurgica 35, 2935–2946.

Adams, B.L., Zhao, J.W., O'Hara, D., 1990. Analysis of interface damage heterogeneity in polycrystalline materials. Acta Metallurgica et Materialia 38, 953–966.

Adams, B.L., Wright, S.I., Kunze, K., 1993. Orientation imaging—the emergence of a new microscopy. Metallurgical Transactions. A, Physical Metallurgy and Materials Science 24, 819–831.

Bartozzi, M., Boyle, A.P., Prior, D.J., 2000. Automated grain boundary detection and classification in orientation contrast images. Journal of Structural Geology 22, 1569–1579.

Bunge, H.J., Weiland, H., 1988. Orientation correlation in grain and phase boundaries. Textures and Microstructures 7, 231–263.

Derby, B., 1990. Dynamic recrystallisation and grain size. In: Barber, D.J., Meredith, P.G. (Eds.), Deformation Processes in Minerals, Ceramics and Rocks. Unwin Hyman, London, pp. 354–364.

Edward, G.H., Etheridge, M.A., Hobbs, B.E., 1982. On the stress dependence of subgrain size. Textures and Microstructures 5, 127–152.

Faul, U.H., Fitz Gerald, J.D., 1999. Grain misorientations in partially molten olivine aggregates: an electron backscatter diffraction study. Physics and Chemistry of Minerals 26, 187–197.

Field, D.P., Adams, B.L., 1992. Interface cavitation damage in polycrystalline copper. Acta Metallurgica et Materialia 40, 1145–1157.

Fliervoet, T.F., White, S.H., Drury, M.R., 1997. Evidence for dominant grain-boundary sliding deformation in greenschist- and amphibolite-grade polymineralic ultramylonites from the Redbank Deformed Zonem, Central Australia. Journal of Structural Geology 19, 1495–1520.

Frese, K., Trommsdorff, V., Kunze, K., 2003. Olivine 100 normal to foliation: lattice preferred orientation in prograde garnet peridotite formed at high H_2O activity, Cima di Gagnone (Central Alps). Contributions to Mineralogy and Petrology 145, 75–86.

Gleason, G.C., Tullis, J., 1993. Improving flow laws and piezometers for quartz and feldspar aggregates. Geophysical Research Letters 20, 2111–2114.

Haessner, F., Pospiech, J., Sztwiertnia, K., 1983. Spatial arrangement of orientations in rolled copper. Materials Science and Engineering 57, 1–14.

Heidelbach, F., Kunze, K., Wenk, H.R., 2000. Texture analysis of a recrystallized quartzite using electron diffraction in the scanning electron microscope. Journal of Structural Geology 22, 91–104.

Heilbronner, R., Tullis, J., 2002. The effect of static annealing on microstructures and crystallographic preferred orientations of quartzites experimentally deformed in axial compression and shear. In: de Meer, S., Drury, M., De Bresser, J.H.P., Pennock, G.M. (Eds.), Deformation Mechanisms, Rheology and Tectonics: Current Status and Future Perspectives. Geological Society Special Publication, vol. 200. Geological Society, London, pp. 191–218.

Hirth, G., Tullis, J., 1992. Dislocation creep regimes in quartz aggregates. Journal of Structural Geology 14, 145–159.

Hughes, D.A., Hansen, N., 1997. High angle boundaries formed by grain subdivision mechanisms. Acta Materialia 45, 3871–3886.

Hughes, D.A., Liu, Q., Chrzan, D.C., Hansen, N., 1997. Scaling of microstructural parameters: misorientations of deformation induced boundaries. Acta Materialia 45, 105–112.

Lassen, N.C.K., 1996. The relative precision of crystal orientations measured from electron backscattering patterns. Journal of Microscopy (Oxford) 181, 72–81.

Lloyd, G.E., Freeman, B., 1994. Dynamic recrystallization of quartz under greenschist conditions. Journal of Structural Geology 16, 867–881.

MacKenzie, J.K., Thompson, M.J., 1957. Some statistics associated with the random disorientation of cubes. Biometrika 44, 205–210.

Means, W.D., 1981. The concept of steady state foliation. Tectonophysics 78, 179–199.

Pennock, G.M., Drury, M.R., Trimby, P.W., Spiers, C.J., 2002. Misorientation distributions in hot deformed NaCl using electron backscattered diffraction. Journal of Microscopy 205, 285–294.

Poirier, J.P., 1985. Creep of Crystals. Cambridge Univ. Press, Cambridge. 260 pp.

Pospiech, J., Sztwiertnia, K., Haessner, F., 1986. The misorientation distribution function. Textures and Microstructures 6, 201–215.

Post, A., Tullis, J., 1998. The rate of water penetration in experimentally deformed quartzite: implications for hydrolytic weakening. Tectonophysics 295, 117–137.

Prior, D.J., 1999. Problems in determining the orientations of crystal misorientation axes, for small angular misorientations, using electron backscatter diffraction in the SEM. Journal of Microscopy 195, 217–225.

Prior, D.J., Trimby, P.W., Weber, U.D., Dingley, D.J., 1996. Orientation contrast imaging of microstructures in rocks using forescatter detectors in the scanning electron microscope. Mineralogical Magazine 60, 859–869.

Prior, D.J., Boyle, A.P., Brenker, F., Cheadle, M.J., Day, A., Lopez, G., Peruzzo, L., Potts, G.J., Reddy, S.M., Spiess, R., Timms, N.O., Trimby, P.W., Wheeler, J., Zetterström, L., 1999. The application of electron backscatter diffraction and orientation contrast imaging in the SEM to textural problems in rocks. American Mineralogist 84, 1741–1759.

Randle, V., 1993. The measurement of grain boundary geometry. Electron Microscopy in Materials Science. Institute of Physics, London. 169 pp.

Saylor, D.M., Morawiec, A., Adams, B.L., Rohrer, G.S., 2000. Misorientation dependence of the grain boundary energy in magnesia. Interface Science 8, 131–140.

Takahashi, M., Nagahama, H., 2000. Fractal grain boundary migration. Fractals - Complex Geometry Patterns and Scaling in Nature and Society 8, 189–194.

Trimby, P.W., Prior, D.J., 1999. Microstructural imaging techniques: a comparison of light and scanning electron microscopy. Tectonophysics 303, 71–81.

Trimby, P.W., Prior, D.J., Wheeler, J., 1998. Grain boundary hierarchy development in a quartz mylonite. Journal of Structural Geology 20, 917–935.

Trimby, P.W., Drury, M.R., Spiers, C.J., 2000. Recognising the crystallographic signature of recrystallisation processes in deformed rocks: a study of experimentally deformed rocksalt. Journal of Structural Geology 22, 1609–1620.

Trimby, P., Day, A., Mehnert, K., Schmidt, N.H., 2002. Is fast mapping good mapping? A review of the benefits of high-speed orientation mapping using electron backscatter diffraction. Journal of Microscopy 205, 259–269.

Urai, J.L., Means, W.D., Lister, G.S., 1986. Dynamic recrystallisation of minerals. In: Hobbs, B.E., Heard, H.C. (Eds.), Mineral and Rock Deformation: Laboratory Studies. Geophysical Monograph, vol. 36. AGU, Washington, DC, pp. 161–199.

Vorhauer, A., Hebesberger, T., Pippan, R., 2003. Disorientations as a function of distance: a new procedure to analyze local orientation data. Acta Materialia 51, 677–686.

Weibel, E.R., 1980. Stereological Methods: Volume 2. Theoretical Foundations. Academic Press, London. 340 pp.

Wheeler, J., 1989. A concise algebraic method for assessing strain in distributions of linear objects. Journal of Structural Geology 11, 1007–1010.

Wheeler, J., Prior, D.J., Jiang, Z., Spiess, R., Trimby, P.J., 2001. The petrological significance of misorientations between grains. Contributions to Mineralogy and Petrology 141, 109–124.

White, S.H., 1977. Geological significance of recovery and recrystallisation processes in quartz. Tectonophysics 39, 143–170.